

Method for determining absolute partial cross sections for radiative and nonradiative deexcitation of metastable hydrogenlike ions

H. T. Schmidt, S. H. Schwartz, A. Fardi, K. Haghghat, and H. Cederquist
Department of Physics, Atomic Physics, Stockholm University, S-104 05 Stockholm, Sweden

L. Liljeby
Manne Siegbahn Laboratory, Stockholm University, S-104 05 Stockholm, Sweden

A. Langereis
Department of Physics, Uppsala University, S-75121 Uppsala, Sweden

J. C. Levin and I. A. Sellin
Department of Physics and Astronomy, University of Tennessee, Knoxville, Tennessee 37996-1200
 (Received 30 April 1998)

In this work we present a method developed to measure separately the radiative and nonradiative contributions to the cross section for collisional deexcitation of metastable hydrogenlike ions. We present the results of the first experiment applying this method, where deexcitation of metastable $\text{He}^+(2s)$ ions in collisions with argon atoms is considered. First the total deexcitation cross section for 6.6 keV $^4\text{He}^+(2s)$ ions is measured absolutely in a beam-gas attenuation experiment. Then the absolute cross section for nonradiative deexcitation is measured separately by coincident detection of projectiles keeping their initial charge state $1+$ and recoil ions (formed only in *nonradiative* deexcitation events). Further, we discuss a semiclassical calculation of the radiative deexcitation cross section, in which the influence of competing electron-capture processes is taken into account in a semiempirical fashion. The result is in agreement with the measured radiative deexcitation cross section of $(5.4 \pm 1.3) \times 10^{-16} \text{ cm}^2$, which amounts to $(70 \pm 8)\%$ of the total deexcitation cross section. [S1050-2947(98)04110-9]

PACS number(s): 34.50.Fa, 32.10.Dk, 52.20.Hv

I. INTRODUCTION

When one or both collision partners in an atomic collision process are in an electronically excited state, excitation energy may be transferred from one to the other. A well-known example of this is a HeNe laser where the upper laser level in the neon atom is populated in a nearly resonant excitation transfer collision between a metastable helium atom and a ground-state neon atom [1]. Other examples of excitation transfer collisions are the so-called energy-pooling collisions where two excited atoms collide and form a final state with one atom highly excited and the other one in the ground state [2–4]. A special situation arises when an excited atom collides with a ground-state atom of a different element with an ionization potential lower than the excitation energy of the excited atom. In this case an excitation transfer collision may lead to ionization of the target. This process is known as Penning ionization and has been the subject of extensive experimental and theoretical investigations since it was first proposed by Penning [5]. Penning ionization in thermal collisions between metastable and ground-state neutral atoms has been reviewed by Hotop [6] and Niehaus [7].

In the 1970s three measurements of the *total* collisional deexcitation cross section for $\text{He}^+(2s)$ ions colliding with various targets at collision energies ranging from near-thermal [8,9] to keV [10] energies were performed. Theoretically, collisional deexcitation of ions was first considered by Lamb in connection with Lamb shift measurements for He^+ ions [11,12]. A calculation of the cross sections for radiative

and nonradiative deexcitation in He^+ -He collisions at thermal energy ($E=23 \text{ meV}$) was performed and it was found that the radiative part constituted 68% of the total deexcitation cross section. In connection with the measurements at sub-eV collision energies of Prior and Wang [8], the rate of radiative deexcitation was calculated by a semiclassical approach, which we also apply in this work. Their comparison of calculated results for radiative deexcitation and measured total deexcitation rates was consistent with zero contribution from nonradiative deexcitation, but with the rather large systematic experimental uncertainties a significant nonradiative contribution could not be excluded [8].

In the present work, we emphasize an experimental method to separately determine the cross sections for radiative and nonradiative deexcitation. As a first test of this technique we consider 6.6 keV $^4\text{He}^+(2s)$ -Ar collisions and determine separately the cross sections for the radiative



and nonradiative



deexcitation processes [13]. $\text{He}^+(2s)$ -Ar collisions are of specific interest in fusion research since $\text{He}^+(2s)$ is formed in abundance in resonant charge exchange in He^{2+} -H colli-

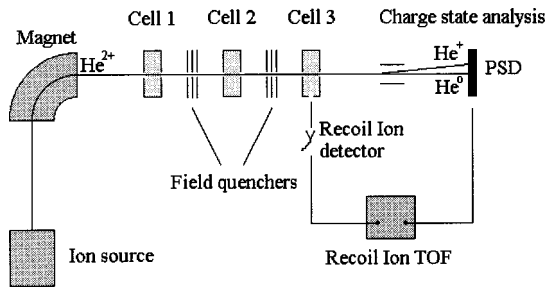


FIG. 1. Schematic of the experimental arrangement.

sions and argon is considered for gas injection at the Tokamak plasma periphery to enhance plasma edge radiation cooling [14].

The mechanism for radiative collisional deexcitation can be described as follows: The target atom is polarized in the electric field of the approaching projectile ion. This induced electric dipole field of the target atom in turn acts on the projectile to Stark mix the $2s$ and $2p$ states. For distances smaller than a few atomic units the Stark splitting exceeds the zero-field $2s_{1/2}$ - $2p_{1/2}$ splitting. For about one femtosecond, the field is sufficiently strong to completely mix the $2s_{1/2}$ and $2p_{1/2}$ levels. After the collision, there is therefore a high probability that the ion is found in the $2p_{1/2}$ state resulting in decay to the ground state on a 100 ps time scale. In the work of Prior and Wang [8], a semiclassical approach is used to derive the cross section for radiative deexcitation. Here, we modify this model by taking into account competing electron-capture mechanisms at small impact parameters. For the present velocity range, the dominating mechanism for *nonradiative* deexcitation is probably electron capture to doubly excited states of the projectile followed by autoionization at large internuclear distance.

In the following section the experimental setup is presented. Section III is concerned with preparatory measurements of the fraction of metastable He^+ ions in the beam and the cross sections for single electron capture in Ar for $\text{He}^+(1s)$ and $\text{He}^+(2s)$ projectiles. In Sec. IV we describe the measurement of the total deexcitation cross section, whereas Sec. V is dedicated to the determination of the cross section for Penning ionization. Finally, in Sec. VI the results are discussed and it is shown that the measured *radiative* deexcitation cross section compares favorably with the result of a semiclassical treatment of $2s$ - $2p$ mixing in the induced Ar dipole field when the fact that electron capture, radiative, and nonradiative deexcitation are exclusive processes at a certain range of impact parameters is taken into account.

II. EXPERIMENTAL SETUP

The experimental setup is shown in Fig. 1. It consists of three movable gas cells of length 38 mm and entrance and exit hole diameters of 1.5 mm and 1.7 mm, respectively. The gas pressures are measured absolutely by means of a Baratron. In the preparation phase of the experiment, the three cells are aligned on a common optical axis, but for the actual measurements the cells are slightly displaced with respect to each other. In this way the charge state of interest can be selected after each cell applying only weak electric fields so that field quenching of the metastable ions is avoided.

In the first of the three gas cells, the He^+ beam is produced by electron capture from krypton to a 6.6 keV $^4\text{He}^{2+}$ ion beam. Roughly 10% of the incoming beam captures an electron and becomes He^+ , and out of these a fraction F_0 (of the order of 10%, see Sec. III) will be in the metastable $2s$ state.

The He^+ beam formed in the first cell is then directed through the second cell where, in the case of the total deexcitation cross-section measurement, a fraction of the metastable ions are deexcited to the ground state in collisions with the target atoms. Before and after this cell the beam passes electric field quenching devices in which the metastable ions can be effectively deexcited to allow for background measurements with all ions in the ground state. The electric field quenchers each consist of three parallel stainless-steel plates with 4 mm diam holes for the beam to pass through. The first and last plates are grounded, whereas the middle one can be put on a negative high voltage V_q . The plate separations are 5 mm. Taking into account the nonuniformity of the fields due to the holes in the plates, the probability for an ion to remain in the $2s$ metastable state after passage through both quenchers was calculated to be less than 2×10^{-4} for $V_q = -1.5$ kV [11].

From the third gas cell recoil ions can be extracted and accelerated onto a Ceratron electron multiplier detector in a single-particle counting mode. After the cell, the projectiles are charge-state analyzed by an electrostatic deflector and a position-sensitive microchannel plate detector with a resistive anode. The charge states of the recoil ions are determined by their time-of-flight as measured by means of the time difference between the arrival of a recoil ion at its detector and the corresponding coincidence signal from the position-sensitive projectile detector. The flight time from the first to the third cell is only 2.4 μs , therefore the spontaneous decay with a lifetime of 1.9 ms [9,15] is negligible compared to the collisional deexcitation in the experiment.

The basic idea of the experiment is to perform two series of measurements, one of which is devoted to a determination of the total collisional deexcitation cross section, $\sigma_{\text{de}}^{\text{tot}}(\text{Ar})$, while the aim of the other measurement series is to determine separately the cross section for nonradiative collisional deexcitation, $\sigma_{\text{de}}^{\text{NR}}(\text{Ar})$. The radiative deexcitation cross section, $\sigma_{\text{de}}^{\text{R}}(\text{Ar})$, is finally obtained by subtraction.

The total deexcitation cross section is measured in the following way: First we identify a collision process in cell 3, which has a high cross section in the case of a metastable projectile but a very low (ideally zero) cross section in the case of a ground-state projectile. We can now record the relative yield of recoil-ion charge-state projectile-ion charge-state coincidences corresponding to this process as a function of the argon pressure in cell 2. We thus obtain an attenuation curve bearing information on the total deexcitation cross section in argon. This method relies on the change in the metastable fraction of the beam entering cell 3 due to deexciting collisions in cell 2. This metastable fraction is, however, also affected by collision processes that cause loss of He^+ ions if the cross sections for these processes are not equal for ground- and metastable-state ions. The by far dominating contribution to this beam loss is electron capture, and in order to derive $\sigma_{\text{de}}^{\text{tot}}(\text{Ar})$ from the measured attenuation cross

section, we need to determine the difference between the total electron-capture cross sections for $\text{He}^+(1s)$ and $\text{He}^+(2s)$ from Ar at 6.6 keV projectile energy. A measurement of these cross sections is described in Sec. III.

The determination of the nonradiative deexcitation cross section (defined as the sum of single and double Penning ionization) is a more straightforward measurement. Cell 2 is not used for this, and the target gas of interest (here Ar) is introduced in cell 3. The cross section for Penning ionization is then determined by calibrating the yield of He^+-Ar^+ coincidences to the target thickness, the detection efficiencies, and the flux of He^+ ions through cell 3. To deduce the Penning ionization cross section for a metastable projectile ion from this measurement, we need to know the (much smaller) single ionization cross section for a ground-state projectile ion and the metastable fraction of the He^+ beam created in cell 1. The ground-state cross section is determined simply by repeating the measurement of the $(\text{He}^+-\text{Ar}^+)$ coincidence rate with the field quenchers on. The more involved problem of determining the initial metastable fraction is treated in the following section.

III. PREPARATORY MEASUREMENTS

A. Determination of the initial metastable fraction F_0

In this subsection it is discussed how to determine the initial metastable fraction F_0 , which results from the electron-capture process ($\text{He}^{2+} + \text{Kr} \rightarrow \text{He}^+ + \dots$) taking place in cell 1. With a beam consisting of a mixture of ground- and metastable-state ions, the measurable quantity for a given collision process, i , will be the effective cross section, $\sigma_{\text{eff}}^i(F)$, which is a function of the metastable fraction F at cell 3:

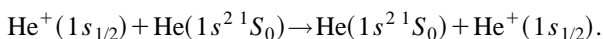
$$\sigma_{\text{eff}}^i(F) = F\sigma_{2s}^i + (1-F)\sigma_{1s}^i, \quad (1)$$

where σ_{1s}^i and σ_{2s}^i are the cross sections for process i (a specific combination of final projectile and target charge states) for $\text{He}^+(1s)$ and $\text{He}^+(2s)$ ions, respectively. Using Eq. (1), we find the following expression for the initial metastable fraction:

$$F_0 = \frac{1 - \sigma_{\text{eff}}^i(F=F_0)/\sigma_{1s}^i}{1 - \sigma_{2s}^i/\sigma_{1s}^i}. \quad (2)$$

For a collision process i with $\sigma_{1s}^i \gg \sigma_{2s}^i$, we find the approximate result $F_0 = 1 - \sigma_{\text{eff}}^i(F=F_0)/\sigma_{1s}^i$. We may thus determine F_0 by measuring σ_{1s}^i and $\sigma_{\text{eff}}^i(F=F_0)$, which corresponds to measurements of the effective cross sections with and without the field quenchers on [see Eq. (1)].

A good candidate for a process for which the cross section is much larger for a $\text{He}^+(1s)$ ion than for a $\text{He}^+(2s)$ ion is electron capture in He, where, in the case of a ground-state projectile ion, there is a strong contribution from the resonant single-capture collision process:



We introduce He in cell 3 and measure the total capture cross sections with and without electric field quenching. Since we only need the ratio of two cross sections to determine F_0 , we

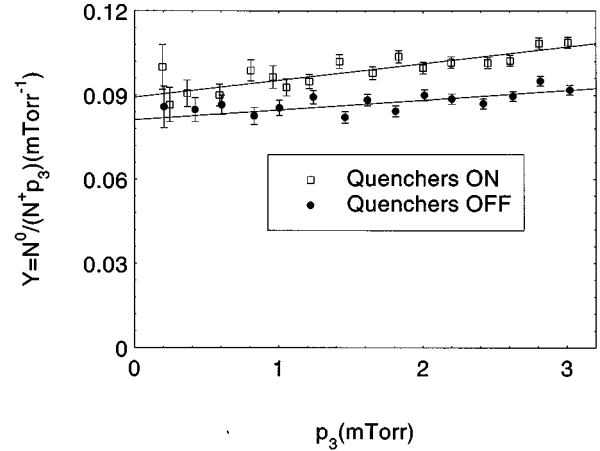


FIG. 2. Normalized yields for electron capture to He^+ from He, Y , defined as the ratio of the number of detected neutralized projectiles, N^0 , to the number of detected projectile ions, N^+ , divided by the He pressure, p_3 , in the third cell are shown as a function of p_3 . By extrapolating to $p_3=0$, effects of multiple collisions are eliminated. The filled circles are data points for the case of a beam with the initial metastable fraction F_0 , while the open squares show data recorded with a pure ground-state beam obtained by electric-field quenching of the metastable beam component.

do not need to worry about systematic effects such as the effective target length, the pressure, and the projectile detection efficiency. We thus only determine the normalized yields, defined as $Y = N^0 / (N^+ p_3)$, where N^0 and N^+ are the numbers of neutrals and ions detected during a certain measuring time and p_3 is the pressure in cell 3 in mTorr. To correct for effects of multiple collisions, we measure Y for a number of different values of p_3 and extrapolate to $p_3=0$. Figure 2 shows Y as a function of p_3 measured with and without the electric field quenchers. For $p_3 \rightarrow 0$, we find $Y^{q\text{ON}}(\text{He}) = 0.0893 \pm 0.0018 \text{ mTorr}^{-1}$ with the quenchers on and $Y^{q\text{OFF}}(\text{He}) = 0.0812 \pm 0.0017 \text{ mTorr}^{-1}$ with the quenchers off. Using Eq. (2), we find the lower limit $F_0 \geq (9.1 \pm 2.6)\%$.

Shah and Gilbody [16] measured F_0 for He^+ beams produced from He^{2+} in collisions with Kr for projectile energies ranging from 3.3 keV/amu to 20 keV/amu. Their technique was based on detection, with known efficiency, of the 304 Å photon emitted when the metastable ions deexcited in an electric field. At their lowest energy point they found $F = (10.0 \pm 1.4)\%$. Since this result is consistent with our lower limit, and since only very little variation with projectile energy was observed, we adopt their lowest energy value and increase the error estimate to 20% and hence choose to use the value $F_0 = (10 \pm 2)\%$ in the following.

B. Determination of total capture cross sections in Ar

The measurement of the total collisional deexcitation cross section to be described in Sec. IV is based on the detection of a change in the metastable fraction of the He^+ beam due to deexcitation in the Ar gas in cell 3. To the extent that the total capture cross sections for ground- and metastable-state ions are not the same, the metastable fraction will also be changed due to the unequal probabilities for $\text{He}^+(1s)$ and $\text{He}^+(2s)$ ions to be neutralized and thereby

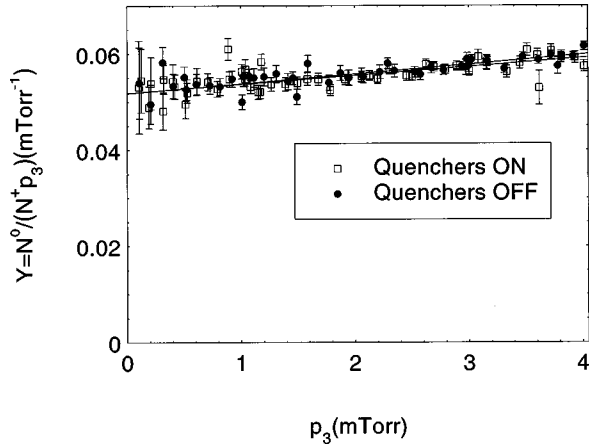


FIG. 3. Normalized yields for electron capture to He^+ from Ar, Y , defined as the ratio of the number of detected neutralized projectiles, N^0 , to the number of detected projectile ions, N^+ , divided by the Ar pressure, p_3 , in the third cell are shown as a function of p_3 . The closed circles are data points for the case of a beam with the initial metastable fraction F_0 , while the open squares show data recorded with a pure ground-state beam obtained by electric-field quenching of the metastable beam component. The difference between the normalized yields with and without field quenching is found to be consistent with zero.

lost from the He^+ beam. To account for this problem we need to determine the total capture cross sections for ground- and metastable-state ions, $\sigma_{1s}^{10}(\text{Ar})$ and $\sigma_{2s}^{10}(\text{Ar})$.

In a manner identical to the one described in the preceding subsection, we determine the normalized yields for electron capture with Ar in cell 3 with and without the field quenchers on. The normalized yields as a function of the Ar pressure, p_3 , are plotted in Fig. 3. Extrapolating to $p_3=0$, we find the results $Y^{q\text{ON}}(\text{Ar})=0.051\,85\pm 0.000\,49\text{ mTorr}^{-1}$ and $Y^{q\text{OFF}}(\text{Ar})=0.051\,77\pm 0.000\,54\text{ mTorr}^{-1}$. The cross sections are proportional to the normalized yield with the factor of proportionality given by $C=(kT/L_3)(\epsilon_{\text{ion}}/\epsilon_{\text{neutral}})$, where k is Boltzmann's constant, $T=293\text{ K}$ is the temperature of the gas, $L_3=(37\pm 5)\text{ mm}$ is the effective target length, and ϵ_{ion} and $\epsilon_{\text{neutral}}$ are the detection efficiencies for He^+ and He^0 at the projectile detector. L_3 is shorter than the geometrical length because of the reduction in pressure in the vicinity of the recoil-ion extraction hole. The uncertainty of L_3 includes a contribution from the estimated error of the pressure measurement.

The ratio of the detection efficiencies can be measured in the following way: The ratio of the total count rate at the detector with a certain pressure in cell 3 and the count rate with no gas in cell 3 is measured many times in order to reduce the influence of beam intensity fluctuations. With gas in cell 3 the apparent charge exchange fraction (found when equal detection efficiencies are assumed) is determined. From this apparent charge exchange fraction and the count rate ratio the true charge exchange fraction as well as the ratio of the efficiencies can be deduced. We thus measured $\epsilon_{\text{ion}}/\epsilon_{\text{neutral}}=1.54\pm 0.11$, where the error is dominated by the influence of varying beam intensity.

Through Eq. (1) we get the difference between the two cross sections, which is what is needed for the measurement of the total deexcitation cross section; $\sigma_{1s}^{10}(\text{Ar})-\sigma_{2s}^{10}(\text{Ar})$

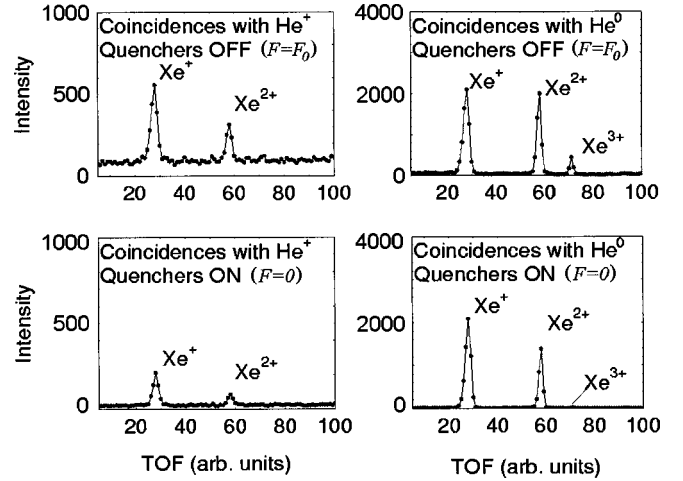


FIG. 4. Time-of-flight spectra recorded with and without the electric-field quenching with xenon in cell 3 in coincidence with He^+ and with He^0 projectiles. The four spectra are recorded for the same integrated beam intensity and the same pressure in cell 3.

$=C/F_0(Y^{q\text{ON}}-Y^{q\text{OFF}})=(1.0\pm 9.2)\times 10^{-17}\text{ cm}^2$, consistent with the two cross sections being equal. Our results for the individual cross sections are $\sigma_{1s}^{10}(\text{Ar})=(6.4\pm 1.0)\times 10^{-16}\text{ cm}^2$ and $\sigma_{2s}^{10}(\text{Ar})=(6.3\pm 1.4)\times 10^{-16}\text{ cm}^2$.

Shah and Gilbody [10] have made very accurate measurements of these cross sections for projectile energies in the range 5–20 keV/amu. At their lowest energy point they found $\sigma_{1s}^{10}=7.3\times 10^{-16}\text{ cm}^2$ and $\sigma_{2s}^{10}=6.1\times 10^{-16}\text{ cm}^2$.

IV. MEASUREMENT OF THE TOTAL DEEXCITATION CROSS SECTION $\sigma_{\text{de}}^{\text{tot}}(\text{Ar})$

The target gas of primary interest (Ar) is introduced in cell 2, where it acts to change the metastable fraction of the He^+ beam (formed in cell 1) mainly by deexcitation collisions. In cell 3 we will then consider a collision process, i , for which $\sigma_{2s}^i \gg \sigma_{1s}^i$, so that i is a good indicator process for metastable ions reaching cell 3.

To identify such a process, we measure with no gas in cell 2 and xenon in cell 3 with and without the electric field quenchers on. Xenon is used in cell 3 because it turns out to be a good indicator for metastable ions emerging from cell 2. We record time-of-flight spectra for recoil ions in coincidence with He^+ ions and in coincidence with He atoms produced in capture collisions in cell 3. This is done both for a beam with the original metastable fraction from the production in cell 1 and with a beam of purely ground-state ions obtained by applying the electric field quenchers. The four resulting time-of-flight spectra are shown in Fig. 4.

From Fig. 4 we find that there are two final charge-state coincidences that have strongly reduced signal strengths when the electric field quenching is applied. These are He^+-Xe^+ , which corresponds to single ionization of the target atom ($i=\text{SI}$), and $\text{He}^0-\text{Xe}^{3+}$, which corresponds to transfer of one electron from the target atom to the projectile ion accompanied by the emission of two additional electrons from the collision process. We refer to the latter process as transfer double ionization ($i=\text{TDI}$).

We introduce Ar in cell 2 and measure the effective cross sections for TDI and SI in cell 3 as a function of the pressure

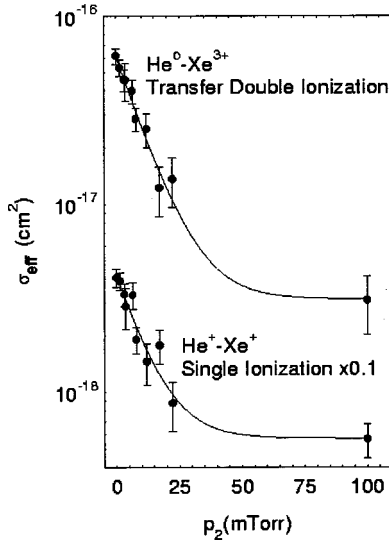


FIG. 5. Effective cross sections, defined as $\sigma_{\text{eff}}^i = F\sigma_{2s}^i + (1 - F)\sigma_{1s}^i$, for single ionization and transfer double ionization as a function of the pressure, p_2 , of argon in cell 2. The measured values of σ_{eff}^i change with p_2 through the change in F caused by deexciting collisions in cell 2. The points at $p_2 = 100$ mTorr are the results of a measurement with the field quenchers on to establish the ground-state contributions to the observed effective cross sections. The full curves are fit curves to extract the total deexcitation cross section.

in cell 2 (0–23 mTorr). Furthermore, the result of the measurement with the field quencher on and therefore no metastables is put in as a data point at high pressure (“ $p_2 = 100$ mTorr”). The effective cross sections as functions of p_2 are plotted in Fig. 5.

To extract the total deexcitation cross section from the data of Fig. 5, we need to consider in detail how the metastable fraction is affected by the collisions with argon atoms in cell 2. From the work of Shah and Gilbody [10], we estimate that the cross section for projectile electron loss from $\text{He}^+(2s)$ is about two orders of magnitude lower than for electron capture. This is corroborated by the fact that we have not been able to observe this process in our measurements. Thus, the processes in cell 2, which affects the metastable fraction, are collisional deexcitation, electron capture to ground-state ions, and electron capture to ions initially in the metastable state. Solving the rate equations when these three processes are taken into account, we find for $\sigma_{1s}^{10} - \sigma_{2s}^{10} \ll \sigma_{\text{de}}^{\text{tot}}$ (valid here) that the metastable fraction after cell 2 is given by

$$F = F_0 \exp\{-[\sigma_{\text{de}}^{\text{tot}} - (\sigma_{1s}^{10} - \sigma_{2s}^{10})]L_2 p_2 / kT\}. \quad (3)$$

By inserting Eq. (3) in Eq. (1), we find the following expression for the effective cross section measured at cell 3 as a function of the argon pressure in cell 2:

$$\sigma_{\text{eff}}^i(\text{Xe}) = A^i \exp(-B p_2) + C^i, \quad (4)$$

where the parameters A^i , B , and C^i are given by

$$A^i = [\sigma_{2s}^i(\text{Xe}) - \sigma_{1s}^i(\text{Xe})]F_0,$$

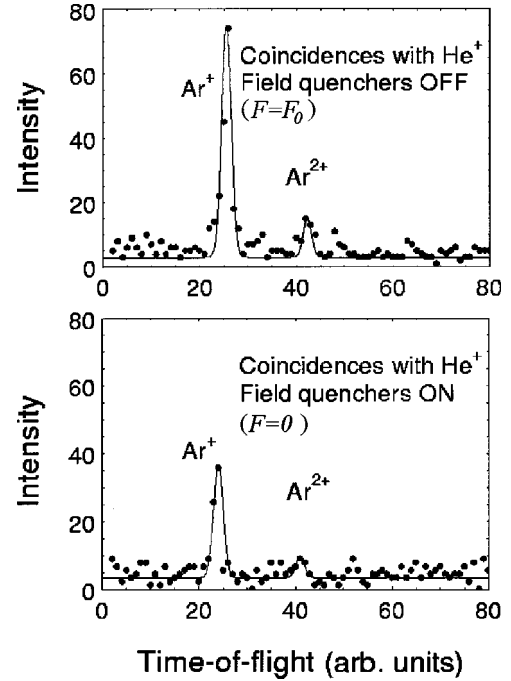


FIG. 6. Time-of-flight spectra showing the pure ionization channels ($\text{He}^+ + \text{Ar} \rightarrow \text{He}^+ + \text{Ar}^{q+} + qe^-$, $q=1,2$) for a beam with the initial metastable fraction and for a beam where the metastables have been field quenched. The spectra are recorded with the same integrated flux of primary ions and the same pressure in cell 3.

$$B = \{\sigma_{\text{de}}^{\text{tot}}(\text{Ar}) - [\sigma_{1s}^{10}(\text{Ar}) - \sigma_{2s}^{10}(\text{Ar})]\}L_2 / kT,$$

$$C^i = \sigma_{1s}^i(\text{Xe}).$$

Note that B , which contains the information of interest, does not depend on the initial metastable fraction F_0 . Nor does it depend on which collision process is considered in cell 3 ($i = \text{SI}$ or $i = \text{TDI}$). We fit Eq. (4) to the two sets of data presented in Fig. 5 by considering A^i , B , and C^i as fitting parameters. In this way we find two independent values for B and thereby for the effective attenuation cross section $\sigma_{\text{att}} = [\sigma_{\text{de}}^{\text{tot}} - (\sigma_{1s}^{10} - \sigma_{2s}^{10})]$. Based on the transfer double ionization data we find $\sigma_{\text{att}}^{\text{TDI}} = (7.35 \pm 1.01) \times 10^{-16}$ cm² and from the single ionization data we find $\sigma_{\text{att}}^{\text{SI}} = (7.90 \pm 1.41) \times 10^{-16}$ cm². As our result we take the weighted average of these two values: $\sigma_{\text{att}} = (7.54 \pm 0.82) \times 10^{-16}$ cm². Using our independent result from Sec. III B [$\sigma_{1s}^{10}(\text{Ar}) - \sigma_{2s}^{10}(\text{Ar}) = (1.0 \pm 9.2) \times 10^{-17}$ cm²], we arrive at the total collisional deexcitation cross section $\sigma_{\text{de}}^{\text{tot}}(\text{Ar}) = (7.6 \pm 1.2) \times 10^{-16}$ cm².

V. MEASUREMENT OF THE CROSS SECTION FOR NONRADIATIVE COLLISIONAL DEEXCITATION $\sigma_{\text{de}}^{\text{NR}}$

To determine the cross section for nonradiative deexcitation (Penning ionization), we make a separate measurement with the same apparatus. We introduce argon in cell 3 to determine the cross sections for single and double ionization for projectile ions in the ground and metastable states (cell 2 is now empty).

In Fig. 6 we show time-of-flight spectra recorded with

argon in cell 3 and in coincidence with projectiles, which remained in charge state $1+$. Data are shown for the two cases with and without the electric field quenching. We find significant rates for both single and double ionization and in both cases the signal is strongest when the field quenching is not applied, showing that the cross sections for these processes are higher for the metastables than for the ground-state ions.

To extract cross sections from the time-of-flight spectra, we need to normalize the integrated peak areas to the incoming beam, the target thickness, and the detection probability of the recoil ions. The detection efficiency for the projectiles does not enter in the determination of the ionization cross sections since the projectiles, which takes part in a ($\text{He}^+ - \text{Ar}^{q+}$) coincidence event, are detected with the same charge and at the same position on the detector as the primary beam.

The detection probability for the recoil ions is determined experimentally as the ratio of the number of neutralized projectiles detected in coincidence with a recoil ion of any charge state to the total number of detected neutralized projectiles. These data are recorded at the same time as the ionization data giving a value for every measurement. A typical result was a detection probability of 2.5% with some fluctuations probably caused by slightly different steering through the third gas cell, but since the efficiency is determined simultaneously with the ionization measurement this does not affect our results. The low value of this detection probability is mainly due to the small length of the extraction aperture of the gas cell compared to the total cell length. Corrections are made for the beam attenuation due to capture in cell 3 and, for the case when the field quenching is not applied, due to deexcitation collisions before the extraction aperture in cell 3.

From the ionization data recorded with the electric field quenchers on, we determine the cross sections for single and double ionization with ground-state ions and find $\sigma_{1s}^{\text{SI}} = (1.39 \pm 0.17) \times 10^{-17} \text{ cm}^2$ and $\sigma_{1s}^{\text{DI}} = (2.75 \pm 1.03) \times 10^{-18} \text{ cm}^2$. From the data without field quenching we extract the effective cross sections for a beam consisting of a mixture of metastable- and ground-state ions with the initial metastable fraction F_0 : $\sigma_{\text{eff}}^{\text{SI}}(F_0) = (3.18 \pm 0.24) \times 10^{-17} \text{ cm}^2$ and $\sigma_{\text{eff}}^{\text{DI}}(F_0) = (5.89 \pm 1.71) \times 10^{-18} \text{ cm}^2$. Using $F_0 = (10 \pm 2)\%$ (see Sec III A) and applying Eq. (1), the cross sections for single and double ionization of the target in a deexcitation collision are found to be $\sigma_{2s}^{\text{SI}} = (1.94 \pm 0.46) \times 10^{-16} \text{ cm}^2$ and $\sigma_{2s}^{\text{DI}} = (3.4 \pm 2.1) \times 10^{-17} \text{ cm}^2$. The sum of the cross sections for these two processes, single and double Penning ionization, gives the nonradiative deexcitation cross section: $\sigma_{\text{de}}^{\text{NR}}(\text{Ar}) = \sigma_{2s}^{\text{SI}} + \sigma_{2s}^{\text{DI}} = (2.3 \pm 0.5) \times 10^{-16} \text{ cm}^2$.

VI. RESULTS AND DISCUSSION

We find the contribution from radiative deexcitation to the total cross section as the difference between the total and nonradiative deexcitation cross sections found in the two preceding sections: $\sigma_{\text{de}}^{\text{R}}(\text{Ar}) = \sigma_{\text{de}}^{\text{tot}}(\text{Ar}) - \sigma_{\text{de}}^{\text{NR}}(\text{Ar}) = (5.4 \pm 1.3) \times 10^{-16} \text{ cm}^2$. Thus the cross section for collision-induced Lyman α emission constitutes $(70 \pm 8)\%$ of the total deexcitation cross section.

In the work of Prior and Wang [8], the rate coefficient for collisional radiative deexcitation of the metastable $2s$ level in one-electron ions is derived from the interaction potential between the approaching ion and the polarizable target atom using straight-line trajectories and applying the sudden approximation [17]. In that work [8], a direct comparison between the experimental result and the result of the derivation was complicated by the fact that the total deexcitation rate was measured and not just the radiative part. Furthermore, there was a broad distribution of collision velocities in the ion trap. In our beam experiment we have a well-defined collision velocity and we determine the cross section for radiative deexcitation separately, and hence these complications are not present. With a well-defined collision velocity the result of Prior and Wang's semiclassical calculation (SCC) can be represented as a formula for the cross section, $\sigma_{\text{de}}^{\text{R}}(\text{SCC})$, when the effect of competing processes is not taken into account:

$$\sigma_{\text{de}}^{\text{R}}(\text{SCC}) = \frac{5}{3} \pi \sqrt{\frac{2\alpha_T \hbar}{Z_p v_p m_e}}, \quad (5)$$

where α_T is the dipole polarizability of the target, m_e is the electron mass, Z_p is the nuclear charge of the projectile, and v_p is the projectile velocity. For 6.6 keV ${}^4\text{He}^+$ on argon $v_p = 5.6 \times 10^5 \text{ m/s}$ and $\alpha_T = 1.64 \text{ \AA}^3$ and hence $\sigma_{\text{de}}^{\text{R}}(\text{SCC}) = 9.6 \times 10^{-16} \text{ cm}^2$. Our experimental result is $\sigma_{\text{de}}^{\text{R}} = (5.4 \pm 1.3) \times 10^{-16} \text{ cm}^2$. The discrepancy is, we believe, due to the fact that the model does not take any competing mechanisms into account. In Sec. III B we found the cross section for electron capture to be $\sigma_{2s}^{10}(\text{Ar}) = (6.3 \pm 1.3) \times 10^{-16} \text{ cm}^2$, which is of the same order of magnitude as the radiative deexcitation cross section. Further, the nonradiative deexcitation will be a non-negligible competing mechanism [$\sigma_{\text{de}}^{\text{NR}}(\text{Ar}) = (2.3 \pm 0.5) \times 10^{-16} \text{ cm}^2$].

In order to provide the means to take the competing mechanisms into account in the comparison between model and experiment, we will consider the derivation of Eq. (5) in more detail. Since the collision time, T , is sufficiently short that \hbar/T by far exceeds the fine-structure splitting of the $n=2$ level of He^+ , the sudden approximation is applicable [8]. In the sudden approximation the probability amplitude, $a_{\nu\mu}$, for going from state μ to state ν during the collision is given by [17]

$$a_{\nu\mu} = \delta_{\nu\mu} - \frac{i}{\hbar} \langle \nu | \int \Delta H(t) dt | \mu \rangle, \quad (6)$$

where $\Delta H(t)$ is the additional term in the Hamilton operator of the projectile ion representing the induced dipole electric field of the target atom. As the projectile velocity is lower than the velocity of the electrons of the target atom, the target electrons have time to adjust to the changing position of the projectile ion, and hence the electric field strength, $|E(t)|$, at the position of the projectile is determined only by the target polarizability, α_T , and the internuclear distance, $R(t)$: $|E(t)| = e\alpha_T/[2\pi\epsilon_0 R(t)^5]$. Assuming straight-line trajectories $R(t) = \sqrt{b^2 + v_p^2 t^2}$, where b is the impact parameter and $R(t)$ takes its minimum value at $t=0$, we thus have

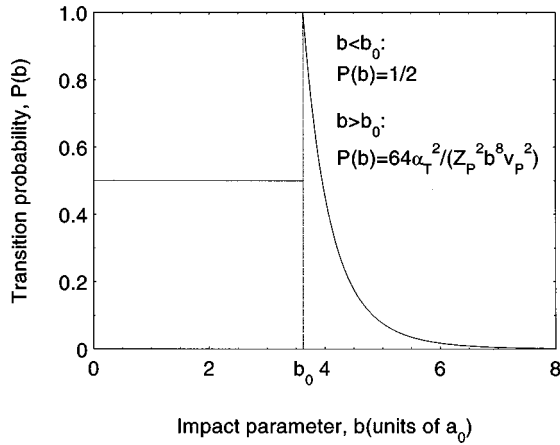


FIG. 7. Transition probability, used in deriving Eq. (5), for a He^+ ion initially in the $2s$ state to be found in the $2p$ state immediately after the collision as a function of the impact parameter.

$$\Delta H(t) = e|E(t)|z = \frac{e^2 \alpha_T z}{2\pi \epsilon_0 (b^2 + v_P^2 t^2)^{5/2}}. \quad (7)$$

The z axis is chosen to point along the internuclear axis and z is the z -coordinate operator of the projectile electron. As the by far dominating contribution to the cross section comes from the region where the Stark shift exceeds the fine-structure splitting, we neglect spin and express the relevant wave functions of the hydrogenlike He^+ ion (ψ_{2s0} and ψ_{2p0}) by the principal, angular orbital, and magnetic quantum numbers. Inserting Eq. (7) in Eq. (6), we then find the probability amplitude for a $2s(m=0) \rightarrow 2p(m=0)$ transition:

$$a_{2p2s} = -\frac{i}{\hbar} \langle \psi_{2p0} | z | \psi_{2s0} \rangle \int_{-\infty}^{\infty} \frac{e^2 \alpha_T}{2\pi \epsilon_0 (b^2 + v_P^2 t^2)^{5/2}} dt. \quad (8)$$

The matrix element is known from text book treatments of the linear Stark effect and is equal to $3a_0/Z_P = 12\pi\epsilon_0\hbar^2/(Z_P m_e e^2)$. Solving the integral of Eq. (8) and taking the modulus square of the resulting probability amplitude, we find an expression for the probability for an incoming $\text{He}^+(2s)$ ion to be in the $2p$ state after the collision, valid for small transition probabilities (i.e., large impact parameters):

$$P(b) = \frac{64}{Z_P^2} \frac{\alpha_T^2 \hbar^2}{b^8 v_P^2 m_e^2}. \quad (9)$$

For *small* impact parameters the wave function will change between $2s(m=0)$ and $2p(m=0)$ many times during the collision. P will therefore oscillate rapidly between zero and unity as a function of b . For sufficiently small values of b we may therefore replace P by the average value and set $P = 1/2$. We follow Prior and Wang [8] and introduce a limiting impact parameter b_0 defined through Eq. (9) by setting $P(b_0) = 1$. For $b < b_0$, we set $P(b) = 1/2$, and for $b > b_0$, Eq. (9) is used. Equation (5) now follows by integrating $2\pi b P(b)$ from zero to infinity. The transition probability used in this integration is plotted as a function of impact parameter in Fig. 7.

For 6.6 keV $^4\text{He}^+$ on Ar the expression in Eq. (9) becomes equal to unity for $b = b_0 = 3.6a_0$. We now assume that the competing processes, electron capture and nonradiative deexcitation, take place for impact parameters smaller than b_0 only. This assumption can be justified by evaluating the distances at which electron transfer can take place, keeping in mind that the nonradiative deexcitation at this energy is assumed to be capture to a doubly excited state followed by autoionization so that both competing processes are electron-transfer processes. According to the classical overbarrier model [18], the distance, R_c , at which electron transfer to a singly charged ion can take place is given by $R_c = 6a_0(I_0/I)$, where I is the ionization potential of the target and I_0 is the ionization potential of atomic hydrogen. For Ar, $I = 15.8$ eV and thus $R_c = 5.2a_0$, which is larger than b_0 . On the other hand, no capture state in He is available 15.8 eV below the energy of $\text{He}^+(2s)$ [the lowest doubly excited state ($2s^2\ ^1S_0$) lies only 7.5 eV below $\text{He}^+(2s)$ and the highest singly excited states converge to $\text{He}^+(1s)$ lying 40.8 eV below $\text{He}^+(2s)$]. Furthermore, for single electron capture to a singly charged ion, the Stark shifts in the initial and final channels cancel exactly, excluding the possibility for this mechanism to provide suitable potential-energy curve crossings at large internuclear distances. This means that electron transfer can only take place at short internuclear distances where the energy levels are strongly perturbed due to overlapping target and projectile electron clouds. At an internuclear distance of $b_0 = 3.6a_0$, this overlap is quite insignificant and we hence conclude that the competing processes mainly are occurring for impact parameters smaller than b_0 .

We may now improve the prediction of Eq. (5) by subtracting half the sum of the measured cross sections for the competing processes. We must subtract only half this sum since $P = 1/2$ for $b < b_0$ so that a projectile, which takes part in a competing process, would have had a 50% chance for collisional radiative deexcitation if it had not taken part in the competing process. This new semiempirical model yields $\sigma_{\text{de}}^R(\text{SEM}) = \sigma_{\text{de}}^R(\text{SCC}) - 0.5(\sigma_{\text{de}}^{\text{NR}} + \sigma_{2s}^{10})_{\text{exp}} = 5.3 \times 10^{-16} \text{ cm}^2$ in agreement with our experimental result $(\sigma_{\text{de}}^R)_{\text{exp}} = (5.4 \pm 1.3) \times 10^{-16} \text{ cm}^2$.

VII. CONCLUSION

We have developed an experimental technique to distinguish between radiative and nonradiative collisional deexcitation of metastable hydrogenlike ions, and applied this technique to the case of $\text{He}^+(2s)$ ions colliding with argon atoms. We find that the radiative deexcitation contributes with $(70 \pm 8)\%$ of the total deexcitation cross section of $\sigma_{\text{de}}^{\text{tot}} = (7.6 \pm 1.2) \times 10^{-16} \text{ cm}^2$. The result for the dominating radiative deexcitation cross section $(\sigma_{\text{de}}^R)_{\text{exp}} = (5.4 \pm 1.3) \times 10^{-16} \text{ cm}^2$ was found to agree with the result of a semiclassical calculation of the $2s$ - $2p$ mixing driven by the induced dipole field of the target atom modified by taking into account competing processes for which the cross sections were measured independently: $\sigma_{\text{de}}^R(\text{SEM}) = \sigma_{\text{de}}^R(\text{SCC}) - 0.5(\sigma_{\text{de}}^{\text{NR}} + \sigma_{2s}^{10})_{\text{exp}} = 5.3 \times 10^{-16} \text{ cm}^2$.

In the work of Prior and Wang [8], no correction for competing mechanisms is performed, hence it is implicitly assumed that any such processes may be neglected at the

very low energies considered in that work. This is consistent with the observation in that work that for a number of targets considered (including Ar and He), the comparison between theory and experiment did not require a nonzero contribution from nonradiative deexcitation. On the other hand, this seems to be in conflict with the earlier calculation by Lamb [11,12], who for 23 meV He⁺-He collisions found the cross section for nonradiative deexcitation to be about half that for radiative deexcitation.

While the mechanism for radiative deexcitation of He⁺(2s) is expected to be the same at thermal and keV energies (field mixing of 2s and 2p), this is not the case for the nonradiative deexcitation via Penning ionization processes. In thermal collisions, the dominant Penning ionization process is autoionization of the quasimolecular collision complex. The collision time is too short for this at keV energies where formation of doubly excited neutral projectile states followed by autoionization after the collision is be-

lieved to be most important. The similarity of the present (70±8% for 6.6 keV He⁺-Ar) and Lamb's result [11,12] (68% for 23 meV He⁺-He) for the radiative branching ratio is thus mildly surprising considering the large difference in collision velocity. Whether this is purely coincidental or if it is an indication of a well-defined velocity scaling also for the nonradiative processes will, hopefully, be revealed by further experiments using the present technique.

ACKNOWLEDGMENTS

This work is supported by the Swedish Natural Science Research Council (Grant Nos. F-GF 08801-315 and F-AA/FU 08801-320), by the Danish Natural Science Research Council (Grant No. 9600989), by the National Science Foundation (Grant No. PHY-9417924), and by the Commission of the European Union (Grant No. ERBFMBICT961754).

-
- [1] A. Javan, W. R. Bennet, and D. R. Herriot, *Phys. Rev. Lett.* **6**, 106 (1961).
- [2] A. N. Klyucharev and A. V. Lazarenko, *Opt. Spectrosc.* **32**, 576 (1972).
- [3] Z. J. Jabbour, R. K. Namiotka, J. Huennekens, M. Allegrini, S. Milosevic, and F. de Tomasi, *Phys. Rev. A* **54**, 1372 (1996).
- [4] S. Guldborg-Kjær, G. De Filippo, S. Milosevic, S. Magnier, J. O. P. Pedersen, and M. Allegrini, *Phys. Rev. A* **55**, R2515 (1997).
- [5] F. M. Penning, *Naturwissenschaften* **15**, 818 (1927).
- [6] H. Hotop, in *Electronic and Atomic Collisions, XI ICPEAC (Kyoto)*, edited by N. Oda and K. Takayanaga (North-Holland, Amsterdam, 1980), p. 271.
- [7] A. Niehaus, *Phys. Rep.* **186**, 149 (1990).
- [8] M. H. Prior and E. C. Wang, *Phys. Rev. A* **9**, 2383 (1974).
- [9] C. A. Kocher, J. E. Clendenin, and R. Novick, *Phys. Rev. Lett.* **29**, 615 (1972).
- [10] M. B. Shah and H. B. Gilbody, *J. Phys. B* **9**, 2685 (1976).
- [11] W. E. Lamb, Jr. and M. S. Skinner, *Phys. Rev.* **78**, 539 (1950).
- [12] E. Lipworth and R. Novick, *Phys. Rev.* **108**, 1434 (1957); W. E. Lamb, Jr. (private communication).
- [13] H. T. Schmidt, S. H. Schwartz, H. Cederquist, L. Liljeby, J. C. Levin, and I. A. Sellin, *Phys. Rev. A* **57**, R4082 (1998).
- [14] See material by R. Janev and D. Schultz (Chap. 11) prepared for *Atomic and Molecular Processes in Fusion Edge Plasmas*, edited by R. Janev (Plenum Press, New York, 1995) and R. Janev (Atomic and Molecular Data Unit, IAEA, Vienna) (private communication).
- [15] M. H. Prior, *Phys. Rev. Lett.* **29**, 611 (1972).
- [16] M. B. Shah and H. B. Gilbody, *J. Phys. B* **9**, 1933 (1976); **7**, 256 (1974).
- [17] L. I. Schiff, *Quantum Mechanics*, 3rd ed. (McGraw-Hill, New York, 1968), p. 292; W. Pauli, *Handbuch der Physik*, Pt. 1, 2nd ed. (Springer, Berlin, 1933), Vol. 24, p. 164.
- [18] A. Bárány, G. Astner, H. Cederquist, H. Danared, S. Hult, P. Hvelplund, A. Johnson, H. Knudsen, L. Liljeby, and K.-G. Rensfelt, *Nucl. Instrum. Methods Phys. Res. B* **9**, 397 (1985).